

# An infinite grid of mesoscopic resistors – investigation and visualization of ballistic conduction

O. Urbański<sup>a</sup>

<sup>a</sup>*Faculty of Physics, Adam Mickiewicz University of Poznań, Uniwersytetu Poznańskiego 2, 61-614 Poznań, Poland*

---

## Abstract

A square lattice of mesoscopic resistors is considered. Each bond is modeled as a narrow waveguide, while junctions are sources of elastic scattering given by a scattering matrix  $\mathbf{S}$ . Symmetry and unitarity constraints are used in a detailed way to simplify all possible matrices  $\mathbf{S}$ . Energetic band structure of the system is determined and visualized for exemplary parameters. Conductance between external electrodes attached to two arbitrary nodes is given by the Landauer formula. Thus the transmittance between the electrodes is calculated. The rest of the paper is devoted to studying wave function patterns arising from an electron injected through one electrode into the system. It is observed that depending on its energy both dull and localized or intricate and expansive patterns occur. It is justified mathematically that fitting electron energy into an energy band can be associated with emergence of complex patterns. Finally, possible experimental realizations of the considered model are briefly mentioned.

*Keywords:* quantum interference effects, ballistic conduction, mesoscopic systems

---

## 1. Introduction

Calculating the net resistance of a network of resistors is a classic and practical school problem. Although larger structures generally demand more computation, periodic and infinite lattices can be handled analytically [1, 2]. In the case of the net resistance measured between adjacent nodes (for uniform lattices), symmetry arguments suffice to determine the answer [1]. For alternating current, resistance can be replaced by impedance, so that the mentioned method applies to an even broader family of circuits.

For arbitrary measuring nodes the problem is more difficult. However, translational symmetry invites one to consider the discrete Fourier transform of relevant quantities (switching to the so-called  $k$ -space). Doing this within the

---

*Email address:* oliwier1459@gmail.com (O. Urbański)

framework of Green's functions yields the net resistance [2]. Current distribution can also be extracted and visualized in a straightforward manner. Figure 1 shows such results for a square and Kagomé lattices obtained by the author using an essentially identical approach to [2].

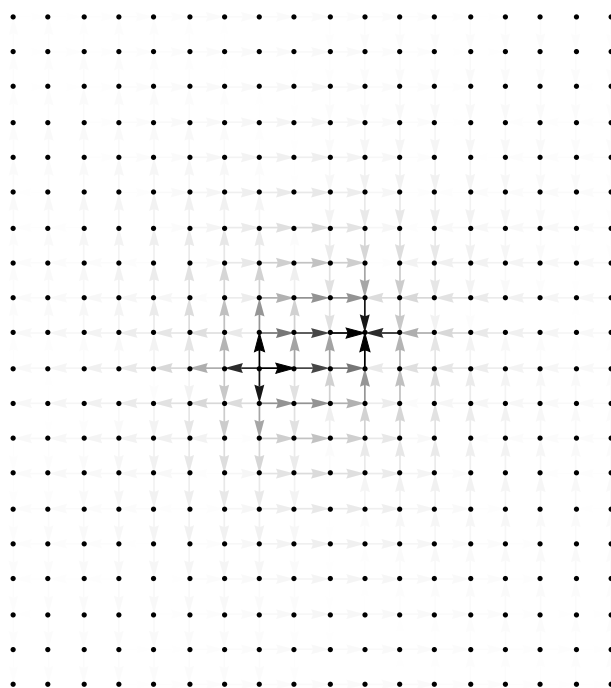
A fundamental assumption present to this point is the Ohm's law. However, it ceases to hold for mesoscopic conductors (i. e. small enough that the mean length of coherence is greater than the conduction path) [3, 4, 5, 6, 7]. Quantum (i. e. interference) effects are of major importance, which modify calculations of the net resistance. In particular, this quantity is no longer additive for series connections [4] and its inverse is not additive for parallel connections [6, 8]. A natural question arises: How do infinite grids of mesoscopic resistors work and are they in any way similar to their classical counterpart?

This question has been partially answered in [8] and [9]. The first work analyzes mesoscopic lattices of resistors to ultimately facilitate quantum percolation, in which wires are randomly deleted. Electrodes are attached to the opposite sides of a large rectangular grid (they extend through an entire length of each side). This slightly differs from the set-up considered in this work. In a full analogy to the classical case (as in Fig. 1), here electrodes are external wires connected to two different nodes. The second mentioned paper focuses on a rectangular lattice with sides  $\ell_1, \ell_2$  and investigates how the energy band structure depends on  $\ell_1/\ell_2$ . Its title emphasizes that this system is a natural generalization of the Kronig-Penney model introduced in [10] to two dimensions. Reference [11] provides a general and detailed treatment of finite counterparts of the considered problem for arbitrary graphs.

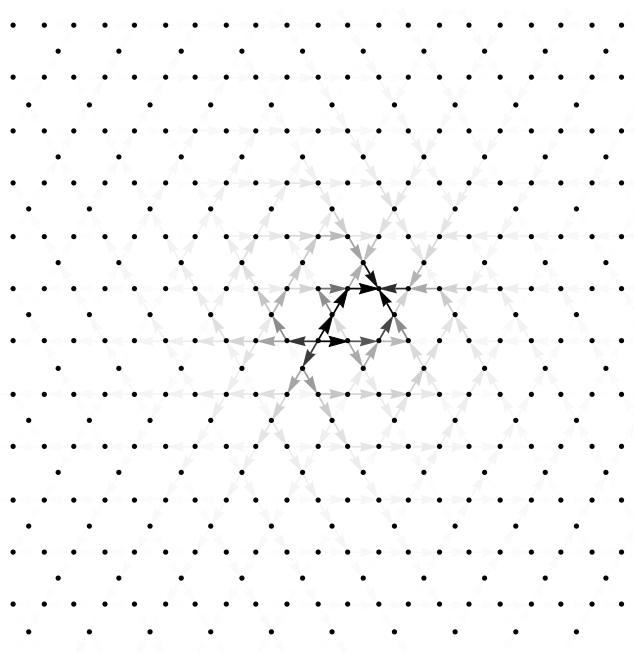
This paper is structured as follows: In Sec. 2 the model for a grid of mesoscopic resistors is described. Sec. 3 shows how basic assumptions allow one to reduce the space of all possible scattering matrices appearing in the model. Sec. 4 presents a calculation of the band-structure, while Sec. 5 tackles the original problem of resistance between the electrodes. It is, however, Sec. 6 which constitutes the heart of this paper, focusing on the features and visualization of the current distribution (or equivalently the wave function pattern). Possible experimental realizations of the considered system are discussed in Sec. 7, ended with a brief summary of the entire work.

## 2. Model

A mesoscopic resistor is modeled as a narrow waveguide, with its transverse dimensions small enough, that the electron motion is essentially one-dimensional. Therefore, only one mode (or channel) of propagation is assumed to be available for the electrons. We consider a square lattice with spacing  $d$  and periodic boundary conditions. Intersections of the wires form centers of scattering, each described by the same scattering matrix  $\mathbf{S}$ . This formulation can account also for scattering sources present in the wires themselves, provided that they are symmetric and identical for every wire. The scattering from a half of every conductor must be incorporated into the scattering matrix corresponding to the closest junction.



(a) Square lattice



(b) Kagomé lattice

Figure 1: Current distribution in infinite grids of classical resistors (arrows indicate direction of the current and their opacity encode its value)

To define  $\mathbf{S}$ , let us consider a single electron wave function propagating in the system. Following [8], in a given wire, it can be given as

$$\psi = Ae^{i\kappa x} + Be^{-i\kappa x}, \quad (1)$$

where  $i$  is the imaginary unit ( $i$  is reserved for indexing lattice sites),  $A$  and  $B$  are complex amplitudes,  $\kappa$  is the Fermi wave number and  $x$  denotes position along the conductor measured from its center. Let  $\mathcal{I}_i$  denote a vector of complex amplitudes of waves incoming from each direction to site  $i$ . Likewise, let  $\mathcal{O}_i$  denote the outgoing amplitudes:

$$\mathcal{I}_i = \begin{pmatrix} \mathcal{I}_{1i} \\ \mathcal{I}_{2i} \\ \mathcal{I}_{3i} \\ \mathcal{I}_{4i} \end{pmatrix}, \quad \mathcal{O}_i = \begin{pmatrix} \mathcal{O}_{1i} \\ \mathcal{O}_{2i} \\ \mathcal{O}_{3i} \\ \mathcal{O}_{4i} \end{pmatrix}. \quad (2)$$

Numbers 1, 2, 3, 4 correspond to four different directions according to the following diagram:

$$\begin{array}{ccccc} & \mathcal{I}_{4i} & \mathcal{O}_{4i} & & \\ & \downarrow & \uparrow & & \\ \mathcal{O}_{1i} & \leftarrow & & \leftarrow & \mathcal{I}_{3i} \\ \mathcal{I}_{1i} & \rightarrow & & \rightarrow & \mathcal{O}_{3i} \\ & \downarrow & \uparrow & & \\ & \mathcal{O}_{2i} & \mathcal{I}_{2i} & & \end{array} \quad (3)$$

Finally,  $\mathbf{S}$  being a  $4 \times 4$  matrix is defined via a relation

$$\mathcal{O}_i = \mathbf{S}\mathcal{I}_i. \quad (4)$$

In order to measure the net resistance between two arbitrary nodes  $i_1$  and  $i_2$ , external electrodes are needed. They inevitably change the scattering at  $i_1, i_2$ , so that two new  $5 \times 5$  scattering matrices  $\mathbf{S}_1$  and  $\mathbf{S}_2$  are needed there. Treating the electrodes as two pins of the entire system, it can be described by a  $2 \times 2$  net scattering matrix

$$\mathbf{S}_{\text{net}} = \begin{pmatrix} r & t \\ t & r \end{pmatrix}. \quad (5)$$

Both electrodes are on equal footing and thus the reflection and transmission amplitudes  $r, t$  are identical for both ways of propagation.

The net conductance  $G$  between the electrodes is given by the Landauer formula [3, 5]. We use its version including the Sharvin contact resistance [7]:

$$G = \frac{e^2}{h} |t|^2. \quad (6)$$

### 3. Unitarity and symmetry constraints on the scattering matrix

[6] gives a full  $3 \times 3$  scattering matrix for a one-to-two symmetric junction (which by assumption does not backscatter). Its form is almost entirely determined by unitarity and spatial symmetry of the system. We want to use such arguments to restrict both  $\mathbf{S}$  and  $\mathbf{S}_1$  ( $\mathbf{S}_2 = \mathbf{S}_1$ ). Starting with  $\mathbf{S}$ , a 4-fold rotary symmetry of each junction, together with an inversion center, enforces the following form:

$$\mathbf{S} = \begin{pmatrix} b & s & f & s \\ s & b & s & f \\ f & s & b & s \\ s & f & s & b \end{pmatrix} e^{i\kappa d}. \quad (7)$$

Factor  $e^{i\kappa d}$  is customary and reflects the phase acquired by traveling the lattice constant.

Elements of matrix  $\mathbf{S}$  depend only on the difference of their indices. For this reason,  $\mathbf{S}$  can be diagonalized by the discrete Fourier transform. Then  $\mathbf{S} = \mathbf{U}^\dagger \mathbf{D} \mathbf{U}$ , where  $\mathbf{U}$  is a unitary matrix representing the discrete Fourier transform and  $\mathbf{D}$  is a complex diagonal matrix. Unitarity is now equivalent to:

$$\begin{aligned} \mathbf{1} &= \mathbf{S} \mathbf{S}^\dagger = \mathbf{U}^\dagger \mathbf{D} \mathbf{D}^\dagger \mathbf{U} = \mathbf{U}^\dagger \mathbf{D} \mathbf{D}^* \mathbf{U} \\ &\Leftrightarrow \mathbf{D} \mathbf{D}^* = \mathbf{1}. \end{aligned} \quad (8)$$

Thus all eigenvalues of  $\mathbf{S}$  must be of unit module, which can be written as:

$$\begin{cases} b + f + 2s &= e^{i\phi_1} \\ b - f &= e^{i\phi_2} \\ b + f - 2s &= e^{i\phi_3} \end{cases}. \quad (9)$$

Solving for  $b, s, f$ , we get:

$$\begin{cases} b = \frac{1}{4} (e^{i\phi_1} + e^{i\phi_3}) + \frac{1}{2} e^{i\phi_2} \\ s = \frac{1}{4} (e^{i\phi_1} - e^{i\phi_3}) \\ f = \frac{1}{4} (e^{i\phi_1} + e^{i\phi_3}) - \frac{1}{2} e^{i\phi_2} \end{cases}. \quad (10)$$

It is interesting that thanks to high symmetry of the scattering potential and unitarity of  $\mathbf{S}$ , we managed to reduce 16 complex matrix elements down to just 3 real phases. Equation (10) implies an interesting inequality, namely  $|s| \leq \frac{1}{2}$ , so  $|s|^2 \leq \frac{1}{4}$ . This means that no more than 25% of electrons get scattered to the right (or left). Taking  $e^{i\phi_2}$  out of the matrix and introducing  $\varphi_1 = \phi_1 - \phi_2$ ,  $\varphi_3 = \phi_3 - \phi_2$ , we obtain:

$$\mathbf{S} = \frac{e^{i(\kappa d + \phi_2)}}{4} \begin{pmatrix} q_+ + 2 & q_- & q_+ - 2 & q_- \\ q_- & q_+ + 2 & q_- & q_+ - 2 \\ q_+ - 2 & q_- & q_+ + 2 & q_- \\ q_- & q_+ - 2 & q_- & q_+ + 2 \end{pmatrix}, \quad (11)$$

where  $q_+ = e^{i\varphi_1} + e^{i\varphi_3}$ ,  $q_- = e^{i\varphi_1} - e^{i\varphi_3}$ . The scattering matrix implicitly used in [8] and [9] (choice referred to as  $\delta$ -coupling with  $\alpha = 0$ ) is obtained by substituting  $\varphi_1 = \pi$ ,  $\varphi_3 = 0$ ,  $\phi_2 = \pi$ . In general, the introduced phases may depend on  $\kappa$ . However, for sufficiently small connections between mesoscopic conductors with comparison to  $2\pi/\kappa$ , we can expect the phases to be essentially independent of  $\kappa$  (which is assumed throughout the rest of the paper).

Scattering matrix  $\mathbf{S}_1$  can be written as a block matrix

$$\mathbf{S}_1 = \begin{pmatrix} \mathbf{S}_1^{\text{red}} & \mathbf{v}_1 \\ \mathbf{w}_1 & (\mathbf{S}_1)_{55} \end{pmatrix}, \quad (12)$$

where  $\mathbf{S}_1^{\text{red}}$  has dimensions  $4 \times 4$ ,  $\mathbf{w}_1$  is  $1 \times 4$  and  $\mathbf{v}_1$  is  $4 \times 1$  (superscript “red” stands for “reduced dimensions”). The fifth index corresponds to the external electrode, which is perpendicular to the lattice. Assuming (similarly to [6]) no backscattering from the electrodes, we can take  $\mathbf{v}_1^T = \mathbf{w}_1 = (\frac{1}{2} \quad \frac{1}{2} \quad \frac{1}{2} \quad \frac{1}{2})$  and  $(\mathbf{S}_1)_{55} = 0$ . Additionally, full symmetry of the remaining four wires leads to

$$\mathbf{S}_1^{\text{red}} = \begin{pmatrix} a_0 & a_1 & a_2 & a_1 \\ a_1 & a_0 & a_1 & a_2 \\ a_2 & a_1 & a_0 & a_1 \\ a_1 & a_2 & a_1 & a_0 \end{pmatrix}. \quad (13)$$

Again, matrix elements of  $\mathbf{S}_1^{\text{red}}$  depend only on the difference of indices. This invites us to use the discrete Fourier transform. Thus, let

$$\mathbf{F} = \begin{pmatrix} \mathbf{F}^{\text{red}} & 0 \\ 0 & 1 \end{pmatrix}, \quad (14)$$

where  $\mathbf{F}^{\text{red}}$  is a  $4 \times 4$  matrix with elements given by:

$$(\mathbf{F}^{\text{red}})_{nm} = \frac{1}{2} e^{-2\pi i \frac{(n-1)(m-1)}{4}}, \quad (15)$$

where  $n, m = 1, 2, 3, 4$ .  $\mathbf{F}$  is a unitary matrix, which satisfies

$$\mathbf{F} \mathbf{S}_1 \mathbf{F}^\dagger = \begin{pmatrix} 2\tilde{a}_0 & 0 & 0 & 0 & 1 \\ 0 & 2\tilde{a}_1 & 0 & 0 & 0 \\ 0 & 0 & 2\tilde{a}_2 & 0 & 0 \\ 0 & 0 & 0 & 2\tilde{a}_1 & 0 \\ 1 & 0 & 0 & 0 & 0 \end{pmatrix}. \quad (16)$$

Sequence  $(\tilde{a}_0, \tilde{a}_1, \tilde{a}_2, \tilde{a}_1)$  is a discrete Fourier transform of sequence  $(a_0, a_1, a_2, a_1)$ .  $\mathbf{F}$  and  $\mathbf{S}_1$  are unitary, so  $\mathbf{F} \mathbf{S}_1 \mathbf{F}^\dagger$  is as well. It implies  $\tilde{a}_0 = 0$ .  $2\tilde{a}_1$  and  $2\tilde{a}_2$  are eigenvalues of  $\mathbf{F} \mathbf{S}_1 \mathbf{F}^\dagger$ , so they must also be the eigenvalues of  $\mathbf{S}_1$ . From this it follows, that they are of unit module:

$$2\tilde{a}_1 = e^{if_1}, \quad 2\tilde{a}_2 = e^{if_2}. \quad (17)$$

Performing the inverse discrete Fourier transform, we get:

$$\begin{cases} a_0 = \frac{1}{2}e^{if_2} \left( \frac{1}{2} + e^{if} \right) \\ a_1 = -\frac{1}{4}e^{if_2} \\ a_2 = \frac{1}{2}e^{if_2} \left( \frac{1}{2} - e^{if} \right) \end{cases}, \quad (18)$$

with  $f = f_1 - f_2$ . Finally:

$$\mathbf{S}_1^{\text{red}} = \frac{e^{if_2}}{2} \begin{pmatrix} \frac{1}{2} + e^{if} & -\frac{1}{2} & \frac{1}{2} - e^{if} & -\frac{1}{2} \\ -\frac{1}{2} & \frac{1}{2} + e^{if} & -\frac{1}{2} & \frac{1}{2} - e^{if} \\ \frac{1}{2} - e^{if} & -\frac{1}{2} & \frac{1}{2} + e^{if} & -\frac{1}{2} \\ -\frac{1}{2} & \frac{1}{2} - e^{if} & -\frac{1}{2} & \frac{1}{2} + e^{if} \end{pmatrix}, \quad (19)$$

which contains only two real phases.

#### 4. Band structure

The kinetic energy of an electron propagating in a waveguide can be written as  $E = \hbar^2 \kappa^2 / 2m + E_0$ .  $m$  stands for the effective mass of an electron and  $E_0$  is the energy associated with transverse behavior of the wave function. Since only one mode is considered, we can fix the energy scale by setting  $E_0 = 0$ . Therefore, determining the band structure (in the absence of external electrodes) requires finding such  $\kappa$  that there exist amplitudes from Eq. (2), which satisfy Eq. (4). One more geometric condition is needed, namely, an outgoing amplitude is simultaneously an incoming amplitude for a neighboring site:

$$\begin{pmatrix} \mathcal{I}_{1i} \\ \mathcal{I}_{2i} \\ \mathcal{I}_{3i} \\ \mathcal{I}_{4i} \end{pmatrix} = \begin{pmatrix} \mathcal{O}_{3(i+(-1,0))} \\ \mathcal{O}_{4(i+(0,-1))} \\ \mathcal{O}_{1(i+(1,0))} \\ \mathcal{O}_{2(i+(0,1))} \end{pmatrix}, \quad (20)$$

where  $i$  is a pair of coordinates labeling a corresponding site. Relations (4) and (20) form a gigantic set of linear equations. Similarly to the classical case, switching to the  $k$ -space may be beneficial, because translationally invariant objects simplify. Thus, let  $\mathcal{I}_k$  and  $\mathcal{O}_k$  represent discrete Fourier transforms of  $\mathcal{I}_i$  and  $\mathcal{O}_i$  respectively, given by:

$$\mathcal{I}_k = \frac{1}{\sqrt{N}} \sum_i \mathcal{I}_i e^{-ik \cdot i}, \quad (21)$$

$$\mathcal{O}_k = \frac{1}{\sqrt{N}} \sum_i \mathcal{O}_i e^{-ik \cdot i}, \quad (22)$$

with  $N$  representing the total number of sites. Now, both Eqs. (4) and (20) take simpler on-site forms (i. e. such that involve only one index of a  $k$ -space lattice site):

$$\mathcal{O}_k = \mathbf{S} \mathcal{I}_k, \quad (23)$$

$$\begin{pmatrix} \mathcal{I}_{1k} \\ \mathcal{I}_{2k} \\ \mathcal{I}_{3k} \\ \mathcal{I}_{4k} \end{pmatrix} = \begin{pmatrix} \mathcal{O}_{3k} e^{-ik_x} \\ \mathcal{O}_{4k} e^{-ik_y} \\ \mathcal{O}_{1k} e^{ik_x} \\ \mathcal{O}_{2k} e^{ik_y} \end{pmatrix}. \quad (24)$$

Equation (24) can be written in a matrix form:

$$\mathcal{I}_k = \mathbf{M}_k \mathcal{O}_k, \quad (25)$$

where

$$\mathbf{M}_k = \begin{pmatrix} 0 & 0 & e^{-ik_x} & 0 \\ 0 & 0 & 0 & e^{-ik_y} \\ e^{ik_x} & 0 & 0 & 0 \\ 0 & e^{ik_y} & 0 & 0 \end{pmatrix}. \quad (26)$$

Joining Eqs. (23) and (25), we get:

$$\mathcal{O}_k = \mathbf{S} \mathbf{M}_k \mathcal{O}_k. \quad (27)$$

Equality (27) means that for every  $k$ ,  $\mathcal{O}_k$  is an eigenvector of  $\mathbf{S} \mathbf{M}_k$  with eigenvalue 1 (or just a zero vector). Matrix  $\mathbf{M}_k$  is both Hermitian and unitary. Scattering matrix is also unitary, so  $\mathbf{S} \mathbf{M}_k$  is as well. Thus its eigenvalues are of the form  $e^{i\phi}$ , for some real number  $\phi$ . If for at least one  $k = k_0$   $\mathbf{S} \mathbf{M}_k$  has at least one eigenvalue equal to 1 (with eigenvector  $\mathcal{O}_{k_0}$ ), then  $\mathcal{O}_i$  being an inverse Fourier transform of  $\mathcal{O}_{k_0} \delta_{kk_0}$  satisfies the initial problem. Therefore, in order to find the spectrum, for every  $k$  (which is non-dimensional quasi-momentum),  $\kappa$  (being the microscopic wave number) should be adjusted so as to match  $e^{i\phi} = 1$ . This gives four branches of dispersion relation (as there are four eigenvalues)  $E_n(k) = \hbar^2 \kappa_n^2(k) / 2m$  ( $n$  indexes branches). These branches, as it turns out, will have subbranches.

Matrix multiplication  $\mathbf{S} \mathbf{M}_k$  gives:

$$\mathbf{S} \mathbf{M}_k = e^{i(\kappa d + \phi_2)} \mathbf{m}_k, \quad (28)$$

where:

$$\mathbf{m}_k = \frac{1}{4} \begin{pmatrix} e^{ik_x}(q_+ - 2) & e^{ik_y}q_- & e^{-ik_x}(q_+ + 2) & e^{-ik_y}q_- \\ e^{ik_x}q_- & e^{ik_y}(q_+ - 2) & e^{-ik_x}q_- & e^{-ik_y}(q_+ + 2) \\ e^{ik_x}(q_+ + 2) & e^{ik_y}q_- & e^{-ik_x}(q_+ - 2) & e^{-ik_y}q_- \\ e^{ik_x}q_- & e^{ik_y}(q_+ + 2) & e^{-ik_x}q_- & e^{-ik_y}(q_+ - 2) \end{pmatrix}. \quad (29)$$

All four eigenvalues of  $\mathbf{m}_k$  are of unit modulus. We can write them as  $e^{iu_n}$ , where  $n$  indexes four real phases. To force the  $n$ -th eigenvalue of  $\mathbf{S} \mathbf{M}_k$  to be 1 (according to Eq. (28)), we have to put:

$$\kappa_n d + \phi_2 = -u_n + 2\pi l. \quad (30)$$



$l$  is an integer which indexes the mentioned subbranches. Equation (30) can be written as:

$$\kappa_{nl} = \frac{-u_n - \phi_2 + 2\pi l}{d}. \quad (31)$$

Calculating  $u_n$  reduces to finding roots of the fourth order characteristic polynomial of matrix  $\mathbf{m}_k$ . This can be done by means of the Ferrari method [12] (which result takes too much space to be written explicitly here) or numerically. However, a simple analytical formula can be found for  $\varphi_3 = -\varphi_1$ . Physically this condition means, that  $b$  and  $f$  are shifted in phase by  $\pi$ , while  $s$  is out of phase by  $\pi/2$  (relative to  $b$  or  $f$ ). Appendix A gives a derivation of the following formula for the dispersion relation:

$$E = \frac{\hbar^2}{2m} \left[ \frac{\pm_1 \arccos \left( \frac{\sigma}{2} \pm_2 \sqrt{\frac{\sigma^2}{4} - p} \right) - \phi_2 + 2\pi l}{d} \right]^2, \quad (32)$$

where

$$\sigma = -\frac{1}{2} (1 - \cos \varphi_1) (\cos k_x + \cos k_y), \quad (33)$$

$$p = \frac{1}{2} [\cos k_x \cos k_y (1 - \cos \varphi_1) - \cos \varphi_1 - 1], \quad (34)$$

$\pm_1$  and  $\pm_2$  are independent plus-minus signs generating four branches and  $l$  is an arbitrary integer giving rise to further subbranches. Figures 2 and 3 show the dispersion relation plots following from Eq. (32) for  $\frac{\hbar^2}{2m} = 1$ ,  $d = 1$ ,  $\phi_2 = 0$  and  $\varphi_1 = \pi/6$ . It is important to note, that the presence of gaps depends on the chosen parameters. For example,  $\varphi_1 = \pi$ ,  $\varphi_3 = 0$ ,  $\phi_2 = \pi$ , corresponding to [8], lead to a gapless spectrum.

## 5. Transmittance between two electrodes

In the previous situation (i. e. without the electrodes), the scattering relation Eq. (4) was the same for every site  $i$ . Here we introduce two electrodes at sites  $i_1$  and  $i_2$ , so that Eq. (4) has to be changed at these sites. Let  $\mathcal{I}_1^{\text{el}}$  and  $\mathcal{O}_1^{\text{el}}$  denote the incoming and outgoing complex amplitude respectively at the first electrode.  $\mathcal{I}_2^{\text{el}}$  and  $\mathcal{O}_2^{\text{el}}$  are defined similarly for the second electrode. The scattering relation takes then the following form:

$$\begin{cases} \begin{pmatrix} \mathcal{O}_{i_1} \\ \mathcal{O}_1^{\text{el}} \end{pmatrix} = \mathbf{S}_1 \begin{pmatrix} \mathcal{I}_{i_1} \\ \mathcal{I}_1^{\text{el}} \end{pmatrix}, & \text{first electrode} \\ \begin{pmatrix} \mathcal{O}_{i_2} \\ \mathcal{O}_2^{\text{el}} \end{pmatrix} = \mathbf{S}_2 \begin{pmatrix} \mathcal{I}_{i_2} \\ \mathcal{I}_2^{\text{el}} \end{pmatrix}, & \text{second electrode} \\ \mathcal{O}_i = \mathbf{S} \mathcal{I}_i, & i \neq i_1, i_2 \end{cases} \quad (35)$$

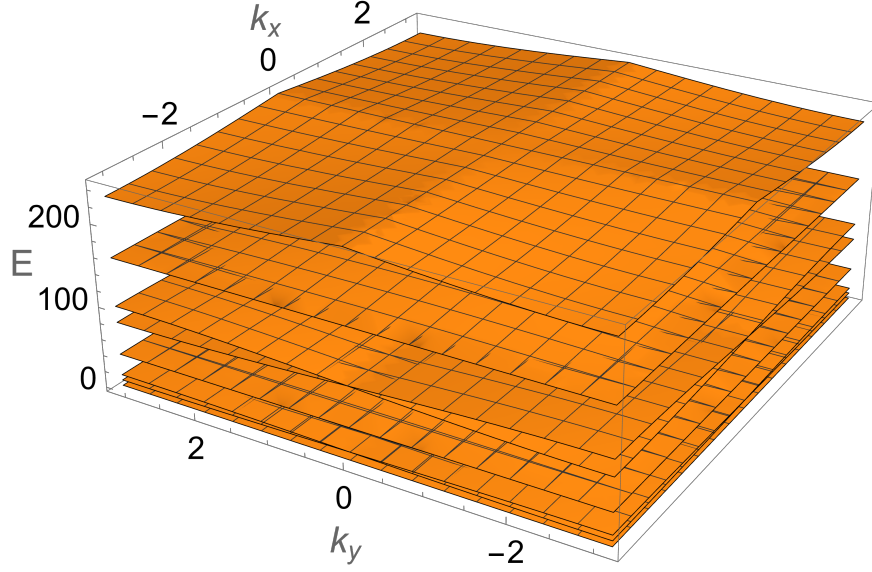


Figure 2: Band structure

Equation (20) remains unchanged and so does Eq. (25).

The goal is to determine the “net scattering matrix”  $\mathbf{S}_{\text{net}}$ , which relates  $(\mathcal{I}_1^{\text{el}}, \mathcal{I}_2^{\text{el}})$  to  $(\mathcal{O}_1^{\text{el}}, \mathcal{O}_2^{\text{el}})$ , by

$$\begin{pmatrix} \mathcal{O}_1^{\text{el}} \\ \mathcal{O}_2^{\text{el}} \end{pmatrix} = \mathbf{S}_{\text{net}} \begin{pmatrix} \mathcal{I}_1^{\text{el}} \\ \mathcal{I}_2^{\text{el}} \end{pmatrix}, \quad (36)$$

together with the field of amplitudes  $\mathcal{I}_i$  and  $\mathcal{O}_i$ . Keeping only the first four components in the first two equations in Eq. (35), we get (using notation introduced in Eq. (12)):

$$\begin{cases} \mathcal{O}_{i_1} = \mathbf{S}_1^{\text{red}} \mathcal{I}_{i_1} + \mathcal{I}_1^{\text{el}} \mathbf{v}_1 & \text{first electrode} \\ \mathcal{O}_{i_2} = \mathbf{S}_2^{\text{red}} \mathcal{I}_{i_2} + \mathcal{I}_2^{\text{el}} \mathbf{v}_2 & \text{second electrode} . \\ \mathcal{O}_i = \mathbf{S} \mathcal{I}_i & i \neq i_1, i_2 \end{cases} \quad (37)$$

Although the full translational symmetry has been spoiled by introducing the electrodes, performing the discrete Fourier transform is still promising. The contribution from sites  $i_1$  and  $i_2$  will break out from the previously encountered regularity, so it has to be handled with special care. Amplitude field  $\mathcal{O}_i$  given by Eq. (37) attains the following form in the  $k$ -space:

$$\begin{aligned} \mathcal{O}_k = \mathbf{S} \mathcal{I}_k + & \frac{(\mathbf{S}_1^{\text{red}} \mathcal{I}_{i_1} + \mathcal{I}_1^{\text{el}} \mathbf{v}_1 - \mathbf{S} \mathcal{I}_{i_1}) e^{-ik \cdot i_1}}{\sqrt{N}} \\ & + \frac{(\mathbf{S}_2^{\text{red}} \mathcal{I}_{i_2} + \mathcal{I}_2^{\text{el}} \mathbf{v}_2 - \mathbf{S} \mathcal{I}_{i_2}) e^{-ik \cdot i_2}}{\sqrt{N}} . \end{aligned} \quad (38)$$

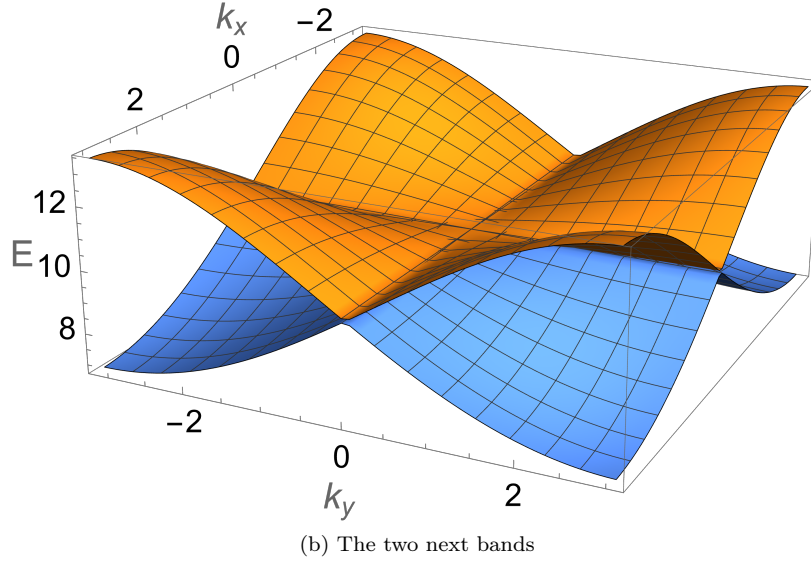
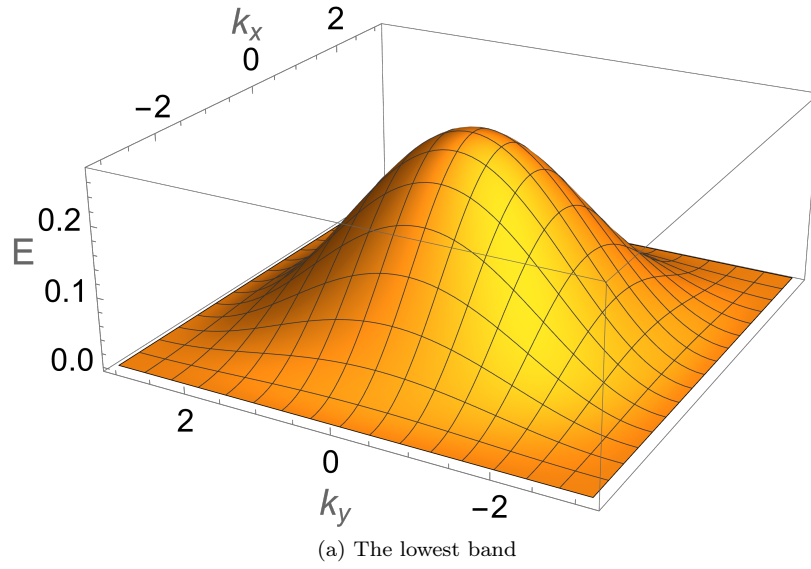


Figure 3: The lowest three bands

Matrix  $\mathbf{M}_k$  given by Eq. (26) is simultaneously Hermitian and unitary and thus it is its own inverse. Thus Eq. (25) can be transformed into

$$\mathcal{O}_k = \mathbf{M}_k \mathcal{I}_k. \quad (39)$$

Without loss of generality we can take  $i_1 = (0, 0)$ . Substituting Eq. (39) to (38) and solving for  $\mathcal{I}_k$ , we get:

$$\begin{aligned} \mathcal{I}_k = \frac{1}{\sqrt{N}} \Big\{ & (\mathbf{M}_k - \mathbf{S})^{-1} [(\mathbf{S}_1^{\text{red}} - \mathbf{S}) \mathcal{I}_{i=0} + \mathcal{I}_1^{\text{el}} \mathbf{v}_1] \\ & + (\mathbf{M}_k - \mathbf{S})^{-1} e^{-ik \cdot i_2} [(\mathbf{S}_2^{\text{red}} - \mathbf{S}) \mathcal{I}_{i_2} + \mathcal{I}_2^{\text{el}} \mathbf{v}_2] \Big\}. \end{aligned} \quad (40)$$

The problem with Eq. (40) is that the incoming amplitudes we want to solve for are present also on the right-hand-side. According to the inverse discrete Fourier transform,  $\mathcal{I}_{i=0} = N^{-1/2} \sum_k \mathcal{I}_k$  and  $\mathcal{I}_{i_2} = N^{-1/2} \sum_k \mathcal{I}_k e^{ik \cdot i_2}$ . Acting on Eq. (40) first with  $N^{-1/2} \sum_k \cdot$  and then with  $N^{-1/2} \sum_k \cdot e^{ik \cdot i_2}$  ( $\cdot$  represents the argument of an operator) we obtain a set of two linear equations for  $\mathcal{I}_{i=0}$  and  $\mathcal{I}_{i_2}$ . Let:

$$\mathbf{R}_i = \frac{1}{N} \sum_k (\mathbf{M}_k - \mathbf{S})^{-1} e^{ik \cdot i}. \quad (41)$$

Now the mentioned system of equations becomes:

$$\begin{cases} \mathcal{I}_{i=0} = & \mathbf{R}_0 [(\mathbf{S}_1^{\text{red}} - \mathbf{S}) \mathcal{I}_{i=0} + \mathcal{I}_1^{\text{el}} \mathbf{v}_1] \\ & + \mathbf{R}_{-i_2} [(\mathbf{S}_2^{\text{red}} - \mathbf{S}) \mathcal{I}_{i_2} + \mathcal{I}_2^{\text{el}} \mathbf{v}_2] \\ \mathcal{I}_{i_2} = & \mathbf{R}_{i_2} [(\mathbf{S}_1^{\text{red}} - \mathbf{S}) \mathcal{I}_{i=0} + \mathcal{I}_1^{\text{el}} \mathbf{v}_1] \\ & + \mathbf{R}_0 [(\mathbf{S}_2^{\text{red}} - \mathbf{S}) \mathcal{I}_{i_2} + \mathcal{I}_2^{\text{el}} \mathbf{v}_2] \end{cases}. \quad (42)$$

Using block matrix notation system of equations (42) can be written as follows:

$$\mathbf{U}_{i_2} \begin{pmatrix} \mathcal{I}_{i=0} \\ \mathcal{I}_{i_2} \end{pmatrix} = \mathcal{I}_1^{\text{el}} \begin{pmatrix} \mathbf{R}_0 \mathbf{v}_1 \\ \mathbf{R}_{i_2} \mathbf{v}_1 \end{pmatrix} + \mathcal{I}_2^{\text{el}} \begin{pmatrix} \mathbf{R}_{-i_2} \mathbf{v}_2 \\ \mathbf{R}_0 \mathbf{v}_2 \end{pmatrix}, \quad (43)$$

where

$$\mathbf{U}_{i_2} = \begin{pmatrix} \mathbf{1} - \mathbf{R}_0 (\mathbf{S}_1^{\text{red}} - \mathbf{S}) & -\mathbf{R}_{-i_2} (\mathbf{S}_2^{\text{red}} - \mathbf{S}) \\ -\mathbf{R}_{i_2} (\mathbf{S}_1^{\text{red}} - \mathbf{S}) & \mathbf{1} - \mathbf{R}_0 (\mathbf{S}_2^{\text{red}} - \mathbf{S}) \end{pmatrix}. \quad (44)$$

Solving (43) leads to:

$$\begin{pmatrix} \mathcal{I}_{i=0} \\ \mathcal{I}_{i_2} \end{pmatrix} = \mathcal{I}_1^{\text{el}} \mathbf{U}_{i_2}^{-1} \begin{pmatrix} \mathbf{R}_0 \mathbf{v}_1 \\ \mathbf{R}_{i_2} \mathbf{v}_1 \end{pmatrix} + \mathcal{I}_2^{\text{el}} \mathbf{U}_{i_2}^{-1} \begin{pmatrix} \mathbf{R}_{-i_2} \mathbf{v}_2 \\ \mathbf{R}_0 \mathbf{v}_2 \end{pmatrix}. \quad (45)$$

Finally, we invoke the first two equations in Eq. (35) and Eq. (12), to express  $\mathcal{O}_1^{\text{el}}$  and  $\mathcal{O}_2^{\text{el}}$  in terms of  $\mathcal{I}_1^{\text{el}}$  and  $\mathcal{I}_2^{\text{el}}$ . This gives:

$$\begin{aligned} \mathbf{S}_{\text{net}} = & \begin{pmatrix} \mathbf{w}_1 & 0 \\ 0 & \mathbf{w}_2 \end{pmatrix} \mathbf{U}_{i_2}^{-1} \begin{pmatrix} \mathbf{R}_0 \mathbf{v}_1 & \mathbf{R}_{-i_2} \mathbf{v}_2 \\ \mathbf{R}_{i_2} \mathbf{v}_1 & \mathbf{R}_0 \mathbf{v}_2 \end{pmatrix} \\ & + \begin{pmatrix} (\mathbf{S}_1)_{55} & 0 \\ 0 & (\mathbf{S}_2)_{55} \end{pmatrix}. \end{aligned} \quad (46)$$

Formula (46) allows calculations of the net scattering matrix, but gives rather a faint insight about its qualitative behavior. This issue is addressed in the next section.

Inverse of the  $\mathbf{U}$  matrix (which is  $8 \times 8$ ) can be expressed in terms of matrix expressions involving its  $4 \times 4$  block matrices [13] (by means of the Schur complement). Although maximal matrix size is decreased, the final formulas are by no means more concise and do not give any additional insight into the problem.

In order to determine  $\mathcal{I}_i$ , we do the inverse Fourier transform on Eq. (40). Substituting for  $\mathcal{I}_{i=0}$  and  $\mathcal{I}_{i_2}$  produces the following recipe:

$$\begin{aligned} \mathcal{I}_i = & \left[ (\mathbf{R}_i (\mathbf{S}_1^{\text{red}} - \mathbf{S}) | \mathbf{R}_{i-i_2} (\mathbf{S}_2^{\text{red}} - \mathbf{S})) \mathbf{U}_{i_2}^{-1} \right. \\ & \left. \times \begin{pmatrix} \mathbf{R}_0 \mathbf{v}_1 & \mathbf{R}_{-i_2} \mathbf{v}_2 \\ \mathbf{R}_{i_2} \mathbf{v}_1 & \mathbf{R}_0 \mathbf{v}_2 \end{pmatrix} + (\mathbf{R}_i \mathbf{v}_1 | \mathbf{R}_{i-i_2} \mathbf{v}_2) \right] \begin{pmatrix} \mathcal{I}_1^{\text{el}} \\ \mathcal{I}_2^{\text{el}} \end{pmatrix}, \end{aligned} \quad (47)$$

where  $(\cdot | \cdot)$  denotes a row block matrix.  $\mathcal{O}_i$  can be found directly from Eq. (47) and Eq. (20).

The obtained formulas extensively use matrix inverses. Therefore, it has been tacitly assumed that these inverses exist. Singularity of  $\mathbf{U}_{i_2}$  would reflect non-uniqueness of  $\mathcal{I}_{i=0}$  and  $\mathcal{I}_{i_2}$  possible due to bound states present in the lattice. This problem does not affect  $\mathbf{S}_{\text{net}}$ . Taking the Moore-Penrose inverse of  $\mathbf{U}_{i_2}$  removes the issue. Singularity of  $\mathbf{M}_k - \mathbf{S}$  for some  $k$  is more problematic, since this matrix appears in Eq. (41) and thus enters  $\mathbf{U}_{i_2}$ . It can be shown that singularity of  $\mathbf{M}_k - \mathbf{S}$  is equivalent to  $\kappa$  corresponding to an energy level from Sec. 4. Namely,  $\det(\mathbf{M}_k - \mathbf{S}) = 0$  is equivalent to

$$0 = \det[(\mathbf{M}_k - \mathbf{S}) \mathbf{M}_k] = \det[\mathbf{1} - \mathbf{S} \mathbf{M}_k], \quad (48)$$

where unitarity of  $\mathbf{M}_k$  has been used. Equation (48) can be rewritten as  $\det[\mathbf{S} \mathbf{M}_k - \lambda \mathbf{1}] = 0$ , with  $\lambda = 1$ , which is exactly the condition found to indicate whether  $\kappa$  corresponds to an existing energy level in a pure lattice (i. e. without external electrodes).

For a finite lattice, the set of allowed energies is discrete, so the set of problematic (i. e. causing  $\det(\mathbf{M}_k - \mathbf{S}) = 0$  for some  $k$ )  $\kappa$  values is of zero measure. This suggests that the problem is rather apparent, although significance of singularity of  $\mathbf{M}_k - \mathbf{S}$  will reappear in the next section.

Figure 4 shows graphically an output of Eq. (47) for  $\varphi_1 = \pi/6$ ,  $\varphi_3 = -\pi/6$ ,  $\phi_2 = 0$ ,  $d = 1$ ,  $\kappa = 5.7$ ,  $f = 0$ ,  $f_2 = \kappa d$ ,  $i_2 = (1, 0)$ ,  $\mathcal{I}_1^{\text{el}} = 1$  and  $\mathcal{I}_2^{\text{el}} = 0$ .

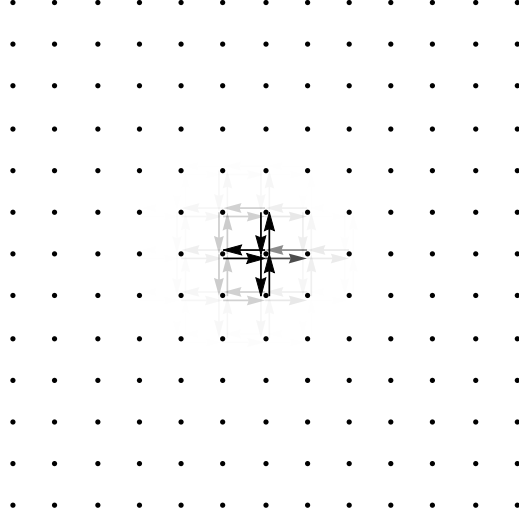


Figure 4: A mesoscopic analog of Fig. 1a. Here, opacity of arrows encodes squared amplitudes of the wave function propagating in the waveguides.

## 6. Wave function patterns

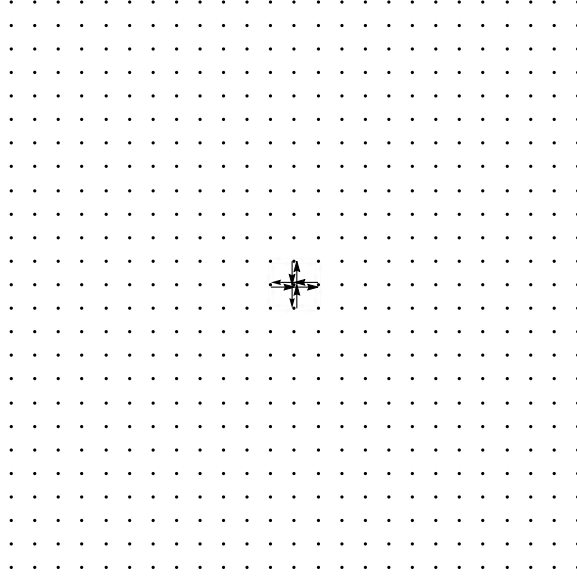
For the investigation of a wave function of a single injected electron, the second electrode is not needed. It introduces additional impurity to the model, which does not seem to be essential for the following observations. Removing that electrode can be achieved by putting  $\mathbf{v}_2 = 0, \mathbf{w}_2 = 0, (\mathbf{S}_2)_{55} = 1$  and  $\mathbf{S}_2^{\text{red}} = \mathbf{S}$ . This allows us to focus on some interesting properties of the current spreading. Matrix  $\mathbf{U}_{i_2}$  reduces significantly and it is no longer needed. Going back to Eq. (42), the system reduces to:

$$\begin{cases} [\mathbf{1} - \mathbf{R}_0 (\mathbf{S}_1^{\text{red}} - \mathbf{S})] \mathcal{I}_{i=0} &= \mathcal{I}_1^{\text{el}} \mathbf{R}_0 \mathbf{v}_1 \\ -\mathbf{R}_{i_2} (\mathbf{S}_1^{\text{red}} - \mathbf{S}) \mathcal{I}_{i=0} + \mathcal{I}_{i_2} &= \mathcal{I}_1^{\text{el}} \mathbf{R}_{i_2} \mathbf{v}_1 \end{cases} \quad (49)$$

Eq. (49) is valid for any  $i_2 \neq 0$ , since after removing the second electrode only site  $i = 0$  is special. Solving for  $\mathcal{I}_{i=0}$  from the first equation, we readily obtain  $\mathcal{I}_{i_2}$  (i. e. the complex amplitude distribution over all sites). Replacing  $i_2 \rightarrow i$ , the formula reads:

$$\begin{aligned} \mathcal{I}_i &= \mathcal{I}_1^{\text{el}} \mathbf{R}_i \\ &\times \left\{ \mathbf{1} + (\mathbf{S}_1^{\text{red}} - \mathbf{S}) [\mathbf{1} - \mathbf{R}_0 (\mathbf{S}_1^{\text{red}} - \mathbf{S})]^{-1} \mathbf{R}_0 \right\} \mathbf{v}_1. \end{aligned} \quad (50)$$

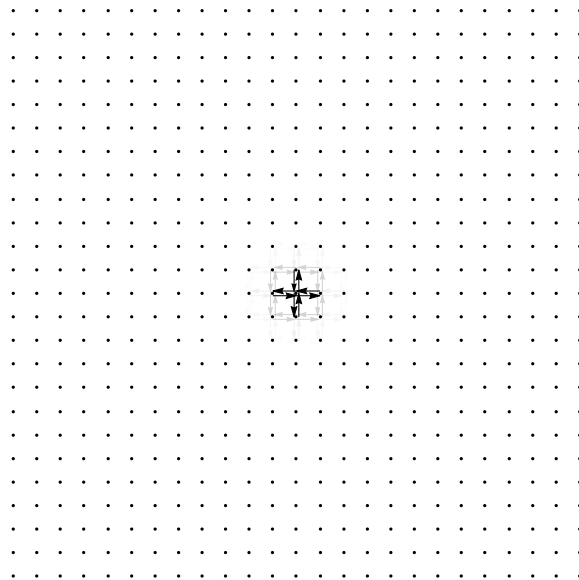
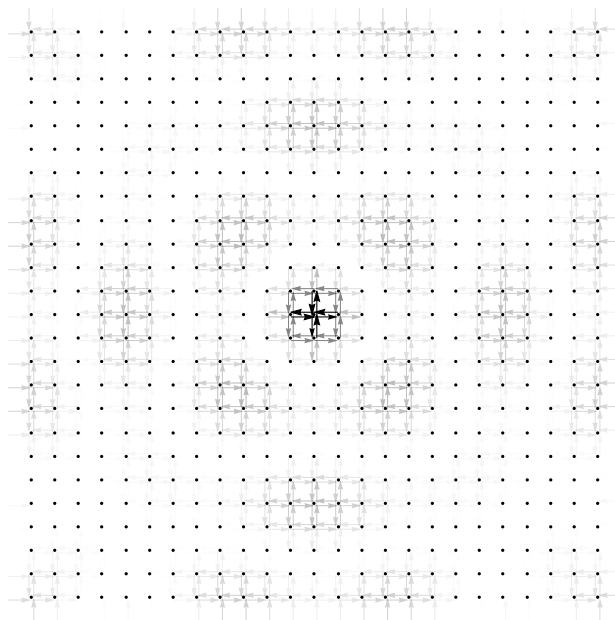
With fixed  $\varphi_1 = \pi/6$ ,  $\varphi_3 = -\pi/6$ ,  $\phi_2 = 0$ ,  $d = 1$ ,  $f = 0$  and  $f_2 = \kappa d$ ,  $\kappa$  was varied and Eq. (50) was used to create patterns in the style of Fig. 4. For the

Figure 5:  $\kappa = 4.3$ 

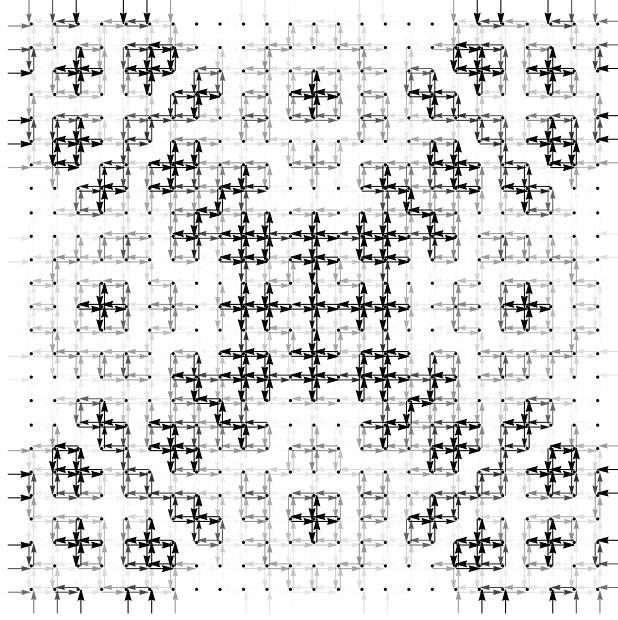
first time, with  $\kappa = 4.3$ , a rather dull structure was observed (Fig. 5). Sadly, it seemed stable upon changing  $\kappa$ . At some point ( $\kappa = 5.7$ , Fig. 6), the current distribution started to grow slightly. Subsequently ( $\kappa = 5.8$ , Fig. 7), significant current appeared far from the electrode – the electron was no longer confined in the small central area. At  $\kappa = 5.9$  (Fig. 8) the electron is completely delocalized. Many different intriguing patterns were observed. Two different examples are given in Fig. 9. Intricate structures persisted until roughly  $\kappa = 6.8$ , when again clear localization around the electrode appeared.

A natural question arises: Can we predict whether a localized or intricate pattern occurs (without determining it in detail)? A formal way of recognizing localized patterns can be by examining the asymptotic behavior of  $\mathcal{I}_i$  as  $i$  tends to infinity. The only site-dependent term in Eq. (50) is  $\mathbf{R}_i$ , so we can focus on asymptotic behavior of its elements.

It is a moment when some clarification regarding the size of the lattice is needed. All condensed-matter physical systems are finite and specifically the grid of mesoscopic resistors has to be as well (moreover, its size must be still much smaller than the coherence length). Therefore, the word “infinite” in the title of this paper means “large”, or more precisely, means that we are interested in some properties formally present in the limit of infinite size. For example, band structure from Fig. 2 and 3 becomes continuous only in this limit (which from now will be referred to as thermodynamic). All wave function visualizations were performed for a finite, but large (namely  $64 \times 64$ ) lattice.

Figure 6:  $\kappa = 5.7$ Figure 7:  $\kappa = 5.8$



Figure 8:  $\kappa = 5.9$ 

A standard thermodynamic limit substitution turning a sum into an integral ( $\frac{1}{N} \sum_k \rightarrow \frac{1}{(2\pi)^2} \int d^2k$ ) leads to the following expression for  $\mathbf{R}_i$ :

$$\mathbf{R}_i = \frac{1}{(2\pi)^2} \int_{-\pi}^{\pi} \int_{-\pi}^{\pi} dk_x dk_y (\mathbf{M}_k - \mathbf{S})^{-1} e^{ik \cdot i}. \quad (51)$$

However, this formula breaks when  $(\mathbf{M}_k - \mathbf{S})^{-1}$  has singularities. Let us first focus on a simpler case, when such singularities do not occur for any  $k \in (-\pi, \pi] \times (-\pi, \pi]$ .

Elements of  $(\mathbf{M}_k - \mathbf{S})^{-1}$  are rational functions of  $e^{ik_x}$ ,  $e^{-ik_x}$ ,  $e^{ik_y}$ ,  $e^{-ik_y}$ . Focusing on just one direction (e. g.  $x$ ), any element of  $\mathbf{R}_i$  can be written as

$$\frac{1}{(2\pi)^2} \int_{-\pi}^{\pi} dk_y I(k_y) e^{ik_y i_y}, \quad (52)$$

where

$$I(k_y) = \int_{-\pi}^{\pi} dk_x \frac{P_{k_y}(e^{ik_x}, e^{-ik_x})}{Q_{k_y}(e^{ik_x}, e^{-ik_x})} e^{ik_x i_x}, \quad (53)$$

with  $P_{k_y}$  and  $Q_{k_y}$  representing some polynomials of  $e^{ik_x}$ ,  $e^{-ik_x}$  with coefficients dependent on  $k_y$ . Introducing a complex variable  $z = e^{ik_x}$ , a  $\int_{-\pi}^{\pi} dk_x$  integral can be exchanged for a complex integral over a unit circle:

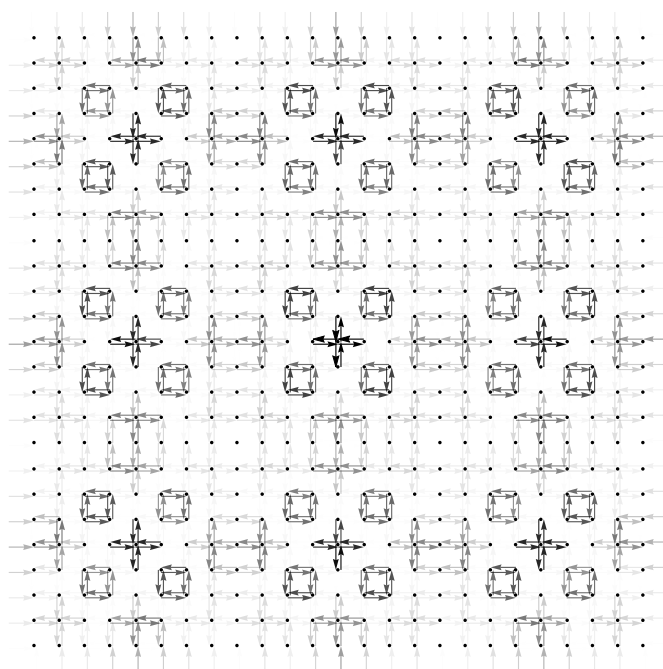
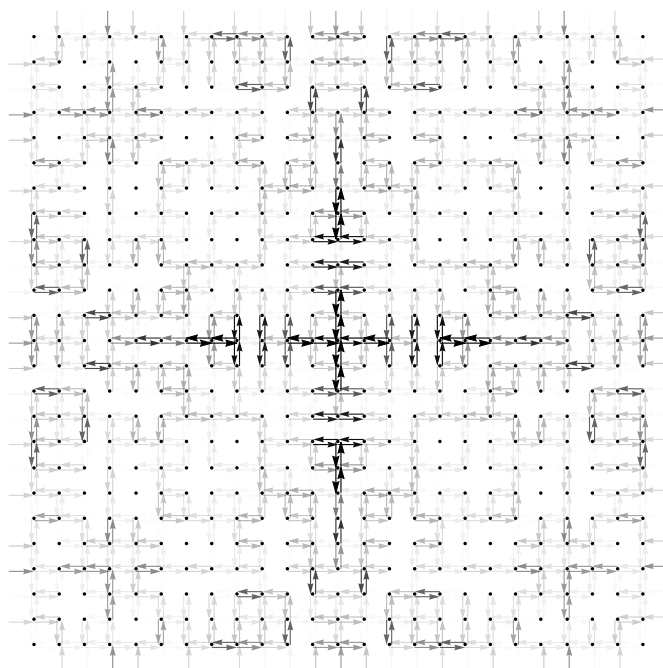
(a)  $\kappa = 6.0$ (b)  $\kappa = 6.2$ 

Figure 9: Two another intricate examples

$$I(k_y) = \oint \frac{dz}{iz} \frac{P_{k_y}(z, z^{-1})}{Q_{k_y}(z, z^{-1})} z^{i_x}. \quad (54)$$

Since  $P$  and  $Q$  are finite bivariate polynomials, there exist such integers  $p$  and  $q$ , that  $z^p P_{k_y}(z, z^{-1}) = \tilde{P}_{k_y}(z)$  and  $z^q Q_{k_y}(z, z^{-1}) = \tilde{Q}_{k_y}(z)$  are polynomials in  $z$  (with no  $z = 0$  roots and also, which can be assumed without loss of generality, no common roots). Thus:

$$I(k_y) = -i \oint dz \frac{\tilde{P}_{k_y}(z)}{\tilde{Q}_{k_y}(z)} z^{i_x+q-p-1}. \quad (55)$$

Polynomial  $\tilde{Q}_{k_y}(z)$  can be factorized as  $\prod_{\ell} (z - z_{\ell})^{m_{\ell}}$  (unless it is constant, but then for sufficiently large  $i_x$  integral  $I$  would be zero).  $\ell$  indexes roots of  $\tilde{Q}$  and  $m_{\ell}$  denotes their multiplicity. By assumption,  $(\mathbf{M}_k - \mathbf{S})^{-1}$  has no singularities, so  $|z_{\ell}| \neq 1$  for all  $\ell$ . Let  $A$  be the set of all such indices  $\ell$  that  $|z_{\ell}| < 1$ . Partitioning the unit circle into many counterclockwise contours (each encircling only one root),  $I$  takes the form

$$\begin{aligned} I(k_y) = -i \sum_{\ell \in A} \oint_{\substack{\text{counterclockwise} \\ \text{contour enclosing} \\ \text{only } z_{\ell}}} dz \\ \times \frac{\tilde{P}_{k_y}(z) / \prod_{\ell' \neq \ell} (z - z_{\ell'})^{m_{\ell'}}}{(z - z_{\ell})^{m_{\ell}}} z^{i_x+q-p-1}. \end{aligned} \quad (56)$$

Using the Cauchy integral formula, we get:

$$\begin{aligned} I(k_y) = \sum_{\ell \in A} \frac{2\pi}{(m_{\ell} - 1)!} \\ \times \left[ \frac{d^{m_{\ell}-1}}{dz^{m_{\ell}-1}} \left( \frac{\tilde{P}_{k_y}(z)}{\prod_{\ell' \neq \ell} (z - z_{\ell'})^{m_{\ell'}}} z^{i_x+q-p-1} \right) \right]_{z=z_{\ell}}. \end{aligned} \quad (57)$$

We are interested in the behavior of  $I$  for  $i_x \gg 1$ . Therefore, focusing only on asymptotic form:

$$I(k_y) \cong \sum_{\ell \in A} c_{\ell} i_x^{m_{\ell}-1} z_{\ell}^{i_x}, \quad (58)$$

where  $c_{\ell}$  are some constants. The main conclusion is, that since  $|z_{\ell}| < 1$  for  $\ell \in A$ ,  $I(k_y)$  (and thus  $\mathbf{R}_i$ ) decays exponentially with  $i_x$ .

It is clear, how the given argument gets spoiled by singularities acquired by  $(\mathbf{M}_k - \mathbf{S})^{-1}$ . They introduce roots  $z_{\ell}$  lying on the unit circle, which ruins complex integral evaluation and also circumvents final observation concerning Eq. (58). In such case, it is not even obvious whether  $\mathbf{R}_i$  approaches anything

in the thermodynamic limit. Fourier transforms of functions with poles may be non-vanishing for  $|i| \rightarrow \infty$ , as exemplified by the principal value of a one dimensional integral  $\int_{-\infty}^{\infty} dk \frac{e^{ikz}}{k} = i\pi$ .

Therefore, intricate patterns (for sufficiently large lattices) can only occur (and generally do occur) when  $(\mathbf{M}_k - \mathbf{S})^{-1}$  (as a continuous function of  $k \in (-\pi, \pi] \times (-\pi, \pi]$ ) has singularities. As justified by Eq. (48), this condition is equivalent to matching a band with the energy of the injected electron. It is possible to derive a closed-form condition for the presence of an intricate pattern, which involves directly the relevant parameters. Details are given in Appendix B.

## 7. Experimental realization and conclusion

Although the entire paper was propelled by the idea of bringing a classical (and classic) infinite grid of resistors to a mesoscopic scale, it is really scattering and interference, that have been truly investigated. Besides this former realization, which is rather hard to achieve, many other systems can be described by the considered model. Instead of an electron wave function, light or acoustic waves could be used.

In the first case, optical fibers can act as quantum wires and four-port star couplers as junctions. The electrodes would be implemented as additional fibers joined to five-port star couplers. Feeding the system with laser light would generate the considered interference pattern inside it. Observing it would require some additional fibers making the light leak out of the grid (i. e. weakly coupled to the system) and shine on a screen. A different alternative might be replacing fibers by free propagation. Then presence of some dust in the air would weakly scatter the light making the intensity distribution directly visible. However, this solution rises technical difficulties with scattering the light by means of star couplers.

In the acoustic case, the mesoscopic grid of resistors gets replaced by a grid of pipes. Visualization of the interference pattern can be achieved by means of the solution from the Rubens tube [14]. Flames besides indicating nodes and antinodes would also characterize the amplitude in the latter.

It should be noted that contributions from different modes (not analyzed in the model) may affect the experiment slightly, as it is the case in multi-mode fiber optics or the classic Rubens tube demonstration.

Waves proved to be promising ornament designers, so it may be an intriguing artistic experience to watch in real time the evolution of the interference pattern. In case of laser light, it would be accompanied by color changes, while in the acoustic case – by pitch changes.

Achieving a transition from an intricate to a localized pattern driven by wavelength changes requires a gapped spectrum. This condition, as seen from Eq. (B.9), depends on phases  $\phi_1, \phi_2, \phi_3$  introduced in Eq. (9). As shown in [8], a gapless spectrum is possible for certain values of these phases, so it is of interest how to avoid such a situation. Phases  $\phi_1, \phi_2, \phi_3$  and  $f_1, f_2$

depend on the detailed geometry of the junctions. It is an interesting question whether any desired values of these can be achieved experimentally, but the answer is not obvious to the author. However, it is sufficient to know if phases generating a gapped spectrum are easily obtainable. The following heuristic argument suggests that it is the case. Considering an almost fully backscattering junctions, parameters from equation (9) are  $b = -1$ ,  $s = f = 0$ . This gives phases  $\phi_1 = \phi_2 = \phi_3 = \pi$ . Then Eq. (B.9) predicts a localized pattern for any  $\kappa$  (excluding a set of zero measure). If a junction unluckily leads to a gapless spectrum, redesigning it for more backscattering should fix the issue. Of course, determining the phases precisely for a given junction would require a separate numerical analysis.

Beyond purely esthetic and educational value, the main finding of the paper, that delocalized intricate interference patterns correspond to fitting the wavelength into a band, could be used to investigate experimentally band structures of similar systems.

### Appendix A. Derivation of the analytical dispersion relation

Assuming  $\varphi_3 = -\varphi_1$ , the characteristic polynomial of matrix  $\mathbf{m}_k$  equated to zero reads:

$$\begin{aligned} & \lambda^4 + (1 - \cos \varphi_1) (\cos k_x + \cos k_y) \lambda^3 \\ & + 2 [\cos k_x \cos k_y (1 - \cos \varphi_1) - \cos \varphi_1] \lambda^2 \\ & + (1 - \cos \varphi_1) (\cos k_x + \cos k_y) \lambda + 1 = 0. \end{aligned} \quad (\text{A.1})$$

All the coefficients are real, so the roots will appear in pairs  $\lambda, \lambda^*$ . Additionally, unitarity of  $\mathbf{m}_k$  enforces all the roots to lie on the unit circle in the complex plane. Thus we can write them as  $e^{iu_1}, e^{-iu_1}, e^{iu_2}, e^{-iu_2}$ . However, if  $\lambda = \pm 1$  was a single root, then its complex conjugate would be identical to it, and the mentioned set of roots would be incomplete. In such case, both  $\lambda = 1$  and  $\lambda = -1$  would have to be roots, because otherwise their total number would be odd. Checking the values of the polynomial at  $\lambda = 1$  and  $\lambda = -1$  gives  $16 \cos^2 \frac{k_x}{2} \cos^2 \frac{k_y}{2} \sin^2 \frac{\varphi_1}{2}$  and  $2(1 - \cos k_x)(1 - \cos k_y)(1 - \cos \varphi_1)$ . Assuming  $\varphi_1 \neq 0$  (and  $\varphi_1 \in (-\pi, \pi]$ ), they can be simultaneously 0 only on a zero-measure subset of the  $k$ -space. Thus we ignore this case and continue assuming all the roots can be written as  $e^{iu_1}, e^{-iu_1}, e^{iu_2}, e^{-iu_2}$ .

Now we can compare the factored form of the characteristic polynomial

$$(\lambda - e^{iu_1})(\lambda - e^{-iu_1})(\lambda - e^{iu_2})(\lambda - e^{-iu_2}), \quad (\text{A.2})$$

with its expanded form (the left-hand-side of Eq. (A.1)). This leads to the following system of equations:

$$\begin{cases} \cos u_1 + \cos u_2 = -\frac{(1 - \cos \varphi_1)(\cos k_x + \cos k_y)}{2} \\ \cos u_1 \cos u_2 = \frac{\cos k_x \cos k_y (1 - \cos \varphi_1) - \cos \varphi_1 - 1}{2} \end{cases} \quad (\text{A.3})$$

Writing it as

$$\begin{cases} x_1 + x_2 &= \sigma \\ x_1 x_2 &= p \end{cases}, \quad (\text{A.4})$$

reveals that its structure is identical to Vieta's formulas for the quadratic equation. Thus  $x_1 = \frac{\sigma}{2} - \sqrt{\frac{\sigma^2}{4} - p}$ ,  $x_2 = \frac{\sigma}{2} + \sqrt{\frac{\sigma^2}{4} - p}$ . Finally:

$$u_1 = \arccos\left(\frac{\sigma}{2} - \sqrt{\frac{\sigma^2}{4} - p}\right), \quad (\text{A.5})$$

$$u_2 = \arccos\left(\frac{\sigma}{2} + \sqrt{\frac{\sigma^2}{4} - p}\right), \quad (\text{A.6})$$

which leads directly to Eq. (32).

### Appendix B. Derivation of the analytical intricacy condition

$(\mathbf{M}_k - \mathbf{S})^{-1}$  has a singularity, when  $\det(\mathbf{M}_k - \mathbf{S}) = 0$ . Symbolic evaluation of the determinant leads to:

$$\begin{aligned} \det(\mathbf{M}_k - \mathbf{S}) &= -e^{i(2d\kappa + \frac{\varphi_1}{2} + \frac{\varphi_3}{2} + 2\phi_2)} \\ &\times \left\{ -2 \cos\left(2d\kappa + \frac{\varphi_1}{2} + \frac{\varphi_3}{2} + 2\phi_2\right) \right. \\ &+ (\cos k_x + \cos k_y) \left[ \cos\left(d\kappa + \frac{\varphi_1}{2} - \frac{\varphi_3}{2} + \phi_2\right) \right. \\ &+ \cos\left(d\kappa - \frac{\varphi_1}{2} + \frac{\varphi_3}{2} + \phi_2\right) \\ &\left. \left. - 2 \cos\left(d\kappa + \frac{\varphi_1}{2} + \frac{\varphi_3}{2} + \phi_2\right) \right] \right. \\ &+ 4 \cos k_x \cos k_y \sin\left(\frac{\varphi_1}{2}\right) \sin\left(\frac{\varphi_3}{2}\right) \\ &\left. + 2 \cos\left(\frac{\varphi_1 - \varphi_3}{2}\right) \right\}. \end{aligned} \quad (\text{B.1})$$

$\det(\mathbf{M}_k - \mathbf{S})$  times  $e^{-i(2d\kappa + \frac{\varphi_1}{2} + \frac{\varphi_3}{2} + 2\phi_2)}$  is a real function of  $k$ , which has the following form:

$$f(k_x, k_y) = A \cos k_x \cos k_y + B (\cos k_x + \cos k_y) + C. \quad (\text{B.2})$$

We show that a global extremum occurs only for  $\sin k_x = \sin k_y = 0$  (assuming  $A \neq B$ ; for  $A = B$  one global extremum is at  $(0, 0)$  and the other extends on the boundary of the  $[-\pi, \pi] \times [-\pi, \pi]$  square). Partial derivatives of  $f$  equated to zero read:

$$\begin{cases} \sin k_x (A \cos k_y + B) = 0 \\ \sin k_y (A \cos k_x + B) = 0 \end{cases} \quad (\text{B.3})$$

The Hessian matrix of  $f$  is given by:

$$H = \begin{pmatrix} -\cos k_x (A \cos k_y + B) & A \sin k_x \sin k_y \\ A \sin k_x \sin k_y & -\cos k_y (A \cos k_x + B) \end{pmatrix}. \quad (\text{B.4})$$

Now all candidates for extrema are examined.

If  $A \cos k_y + B = 0$  or  $A \cos k_x + B = 0$ , then  $\det H = -A^2 \sin^2 k_x \sin^2 k_y$ . If both  $\sin k_x$  and  $\sin k_y$  are nonzero, then  $\det H < 0$  and this corresponds to a saddle-point. If exactly one of  $\sin k_x$  and  $\sin k_y$  is zero, let us say  $\sin k_x$ , then  $f$  becomes a linear function of  $\cos k_y$  having an extremum at  $k_y = 0$  or  $k_y = \pm\pi$  (so  $\sin k_x = \sin k_y = 0$ ).

If  $A \cos k_y + B \neq 0$  and  $A \cos k_x + B \neq 0$ , then Eq. (B.3) enforces that  $\sin k_x = \sin k_y = 0$ .

For  $\sin k_x = \sin k_y = 0$  we have to consider only  $k$  being 0 or  $\pi$  (since  $-\pi$  and  $\pi$  are equivalent).

It turns out that:

$$\begin{aligned} & -\frac{e^{-i(2d\kappa + \frac{\varphi_1}{2} + \frac{\varphi_3}{2} + 2\phi_2)}}{16} \det(\mathbf{M}_{(0,0)} - \mathbf{S}) \\ &= \cos^2\left(\frac{d\kappa + \phi_2}{2}\right) \sin\left(\frac{d\kappa + \varphi_1 + \phi_2}{2}\right) \\ &\times \sin\left(\frac{d\kappa + \varphi_3 + \phi_2}{2}\right), \end{aligned} \quad (\text{B.5})$$

$$\begin{aligned} & -\frac{e^{-i(2d\kappa + \frac{\varphi_1}{2} + \frac{\varphi_3}{2} + 2\phi_2)}}{16} \det(\mathbf{M}_{(\pi,\pi)} - \mathbf{S}) \\ &= \sin^2\left(\frac{d\kappa + \phi_2}{2}\right) \cos\left(\frac{d\kappa + \varphi_1 + \phi_2}{2}\right) \\ &\times \cos\left(\frac{d\kappa + \varphi_3 + \phi_2}{2}\right), \end{aligned} \quad (\text{B.6})$$

$$\begin{aligned} & -\frac{e^{-i(2d\kappa + \frac{\varphi_1}{2} + \frac{\varphi_3}{2} + 2\phi_2)}}{16} \det(\mathbf{M}_{(0,\pi)} - \mathbf{S}) \\ &= \frac{1}{4} \sin(d\kappa + \phi_2) \sin\left(d\kappa + \frac{\varphi_1}{2} + \frac{\varphi_3}{2} + \phi_2\right). \end{aligned} \quad (\text{B.7})$$

According to Eq. (B.1),

$$-\frac{1}{16} \det(\mathbf{M}_k - \mathbf{S}) e^{-i(2d\kappa + \frac{\varphi_1}{2} + \frac{\varphi_3}{2} + 2\phi_2)} \quad (\text{B.8})$$

is a real function of  $k$ , being of the form given by Eq. (B.2). All candidates for global extrema are:

$$\begin{cases} \cos^2\left(\frac{d\kappa + \phi_2}{2}\right) \sin\left(\frac{d\kappa + \varphi_1 + \phi_2}{2}\right) \sin\left(\frac{d\kappa + \varphi_3 + \phi_2}{2}\right) \\ \sin^2\left(\frac{d\kappa + \phi_2}{2}\right) \cos\left(\frac{d\kappa + \varphi_1 + \phi_2}{2}\right) \cos\left(\frac{d\kappa + \varphi_3 + \phi_2}{2}\right) \\ \frac{1}{4} \sin(d\kappa + \phi_2) \sin\left(d\kappa + \frac{\varphi_1}{2} + \frac{\varphi_3}{2} + \phi_2\right) \end{cases} . \quad (\text{B.9})$$

All values taken by Eq. (B.8) belong to the interval between the smallest and the biggest number from Eq. (B.9). Thus the condition for  $\det(\mathbf{M}_k - \mathbf{S})$  to be 0 for some  $k$ , is that not all the values in (B.9) be of the same sign (unless they are all zero). Therefore, this is the condition (which is strictly speaking a necessary condition) for the intricacy of the wave function.

## References

- [1] P. M. Osterberg and A. S. Inan, “Impedance between adjacent nodes of infinite uniform D-dimensional resistive lattices,” *Am. J. Phys.* 72 (7), 972-973 (2004).
- [2] J. Cserti, “Application of the lattice Green’s function for calculating the resistance of an infinite network of resistors,” *Am. J. Phys.* 68 (10), 896-906 (2000).
- [3] R. Landauer, “Spatial variation of currents and fields due to localized scatterers in metallic conduction,” *IBM Res. Dev.* 1 (3), 223-231 (1957).
- [4] R. Landauer, “Electrical resistance of disordered one-dimensional lattices,” *Philos. Mag.* 21 (172), 863-867 (1970).
- [5] M. Büttiker et al., “Generalized many-channel conductance formula with application to small rings,” *Phys. Rev. B* 31 (10), 6207 (1985).
- [6] Y. Gefen, Y. Imry, and M. Ya. Azbel, “Quantum oscillations and the Aharonov-Bohm effect for parallel resistors,” *Phys. Rev. Lett.* 52 (2), 129 (1984).
- [7] M. Büttiker, “Transmission, reflection and the resistance of small conductors,” in *Electronic Properties of Multilayers and Low-Dimensional Semiconductor Structures*, edited by J. M. Chamberlain, L. Eaves, and J.-C. Portal (Plenum Press, New York and London, 1989), p. 51-55.
- [8] Y. Avishai and J. M. Luck, “Quantum percolation and ballistic conductance on a lattice of wires,” *Phys. Rev. B* 45 (3), 1074 (1992).



- [9] P. Exner, “Lattice Kronig-Penney models,” *Phys. Rev. Lett.* 74 (18), 3503 (1995).
- [10] R. de L. Kronig and W. G. Penney, “Quantum mechanics of electrons in crystal lattices,” *Proc. R. Soc. London, Ser. A* 130 (814), 499-513 (1931).
- [11] T. Kottos, U. Smilansky, “Quantum graphs: a simple model for chaotic scattering,” *J. Phys. A: Math. Gen.* 36, 3501 (2003).
- [12] M. Abramowitz, I. A. Stegun (Eds.), “Solutions of Quartic Equations,” §3.8.3 in *Handbook of Mathematical Functions with Formulas, Graphs, and Mathematical Tables*, 9th printing, New York: Dover, pp. 17-18 (1972).
- [13] S. Boyd, L. Vandenberghe, “Convex Optimization,” Cambridge University Press (Appendix A.5.5), (2004).
- [14] K. L. Gee, “The Rubens tube,” *Proc. Meet. Acoust.* 8 (1), (2009).